Electronic Supporting Information for:

pH-Dependent Structure of Water-Exposed Surfaces of CdSe Quantum Dots

Dana Emily Westmoreland[†], Rikkert J. Nap[‡], Francesca Arcudi[†], Igal Szleifer[†‡], and Emily A. Weiss*[†]

[†]*Department of Chemistry, Northwestern University, 2145 Sheridan Rd., Evanston, IL 60208-3113*

[‡]*Department of Biomedical Engineering and Chemistry of Life Processes Institute, Northwestern University, Evanston, IL 60208-3113*

*corresponding author. Email: e-weiss@northwestern.edu

TABLE OF CONTENTS

1. MATERIALS

All chemicals and solvents were purchased from Aldrich and used as received except otherwise indicated with the exception of concentrated HNO_3, which was purchased from Fischer.

2. SYNTHESIS OF QUANTUM DOTS

We used a previously described synthesis to prepare CdSe QDs[2] capped with oleate ligands. We began by synthesizing cadmium oleate from 99.99% trace metals grade cadmium oxide (0.225 g, 1.75 mmol) and 90% technical grade oleic acid (6.3 mL, 22.3 mmol) in 90% technical grade octadecene (13.7 mL, 42.8 mmol) in a dry, 50-mL three-neck round-bottom flask. We heated this mixture to 260°C under an N_2 atmosphere while stirring until the mixture had turned from brown to clear. We then reduced the temperature to ~120°C and opened the flask to the atmosphere while flowing with N_2 for ~30 minutes to remove water formed during the cadmium oleate synthesis.

To synthesize the CdSe QDs, we added the cadmium oleate synthesized in the first step (8 mL) to a 50-mL three-neck round-bottom flask that also contained 99.9% trace metals grade SeO_2 (0.09 g, 0.81 mmol) and 90% technical grade octadecene (12 mL). Under an N_2 atmosphere, we heated the reaction mixture to 240°C with vigorous stirring, since the SeO_2 is only moderately soluble at lower temperatures. The QDs began to form at 210°C when the reaction began to turn orange, and we allowed the temperature to increase to 240°C until the desired size was reached. We purified the QDs by washing first with 3:1 (v/v) methanol:QD solution and centrifuging at 3500 rpm for 5 minutes. We then poured off the supernatant and resuspended the QD pellet in hexanes. We washed the QDs twice more with 3:1 (v/v) acetone:QDs in hexanes and centrifuged as initially, resuspending in hexanes between washes. Finally, we resuspended the QDs in hexanes and stored in the dark. The described purification procedure was adapted from a previous report.[3]

3. LIGAND EXCHANGE PROCEDURE

We added either 30 µL (150 equivalents of per QD) of 0.1 M HCl or 60 µL (300 equivalents per QD) of 0.1 M MPA or PPA in isopropanol (IPA) to a 4 mL solution of 5 µM oleate-capped CdSe QDs in hexanes. We have determined, through ground state absorption spectroscopy, that the number of equivalents of acid needed to ensure colloidal stability of the particles in water differs for HCl, MPA, and PPA, but that not all equivalently strong acids result in phase transfer (**Figure S1**). We therefore suspect that the affinity of the conjugate base for the QD surface in hexanes plays a role in the effectiveness of the phase transfer.The QDs precipitated from hexanes and we resuspended in a 0.3:1 (v/v) mixture of DMF:hexanes (a DMF volume of 1.2 mL). We then removed the hexanes layer by pipette and removed O_2 from the DMF suspension by cycling vacuum followed by flushing with N_2. While the solution was under a N_2 atmosphere, we added 10 mM aqueous KOH to achieve a pH of ~7 (one equivalent KOH

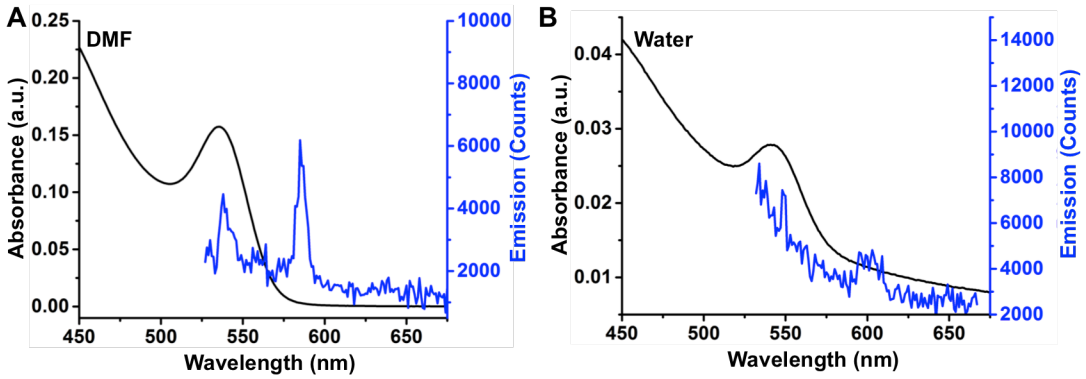

Figure S1. A) Ground state absorption (black) and photoluminescence (blue) spectra of CdSe QDs transferred into DMF using 150 equivalents of HNO_3 per QD. The [QDs] in the DMF layer is 25.6 µM, an essentially quantitative yield of phase transfer. **B)** Ground state absorption (black) and photoluminescence (blue) spectra of CdSe QDs transferred into water using 150 equivalents of HNO_3 per QD. The [QDs] in the DMF layer is 0.5 µM, a yield of 4.6% from DMF.

vs. HCl or MPA, two equivalents of KOH vs. PPA) and then added deionized water to achieve a total water volume of 2.4 mL and a final water to DMF ratio of 2:1 (v/v). This step ensured that the QDs were adequately diluted in the final aqueous solution such that they did not precipitate due to concentration effects. We mixed the solution rapidly under a N_2 atmosphere, and extracted the DMF using two 50-mL $CHCl_3$ washes. We bubbled the resulting water solution briefly with N_2 to evaporate residual $CHCl_3$.

4. APPARATUS AND METHODS

4.1 Ground-State Absorption and Photoluminescence Spectroscopy

We acquired all ground state absorption spectra on a Varian Cary 5000 spectrometer in a 1 cm quartz cuvette in the indicated solvent. We corrected for the baseline of all spectra using a neat solvent sample. We acquired all photoluminescence spectra with a Fluorolog-3 spectrofluorometer (Horiba Jobin Yvon) in a 1 cm quartz cuvette with a 2-nm slit width, and a right angle geometry. The excitation wavelength was 450 nm for all CdSe QD samples. For the photoluminescence measurements, we diluted all samples such that their absorbance at the excitation wavelength was less than 0.1 in order to minimize reabsorption of emission.

4.2 Nuclear Magnetic Resonance Spectroscopy (NMR)

We acquired all ^1H NMR spectra in 80/20 (v/v) H_2O/D_2O on a Bruker Neo 600 MHz spectrometer with a QCl-F cryoprobe using a solvent suppression pulse sequence (4 scans with a relaxation delay time of 2 sec for standard ^1H NMR, 16 scans with a relaxation delay time of 30 sec for solvent suppression ^1H NMR).

4.3 Inductively-Coupled Plasma-Optical Emission Spectroscopy

We centrifuged 400 µL of HCl- and 800 µL of PPA-exchanged QD samples in water at 7000 rpm for 15 minutes and washed the precipitated QD samples three times with water. We then digested the HCl- and PPA-exchanged QD samples in water with 1% nitric acid (aq.) at a 10 mL final volume. We prepared ICP-OES standards at concentrations of 0.1 ppm, 1 ppm, 10 ppm, 25 ppm, and 50 ppm of both cadmium (using a stock solution of 1000 mg/L Cd, Aldrich) and selenium (using a stock solution of 1000 mg/L Se, Aldrich) with 1% nitric acid (aq.) at a 10 mL total volume. We used a Thermo iCAP 7600 ICP-OES instrument to obtain the ICP-OES data and calculated the cadmium and selenium concentrations using the average of the calibrated intensities of the cadmium (228.802, 226.502, 214.438 eV) and selenium (196.090, 203.985, 206.279 eV) atomic emission peaks.

4.4 X-ray Photoelectron Spectroscopy (XPS)

We prepared XPS samples by drop-casting solutions of QDs in water onto Au/Si/SiO2 wafers in a nitrogen box. We transferred the samples to the XPS using an air-free transport vessel. We collected XPS using a Thermo Scientific ESCALAB 250Xi spectrometer with an aluminum anode (1486.6 eV) at 225 W. The dwell time for each sample was 50 msec and 20 scans were collected for Cd. No scans were collected for Se because the Au 3d peaks obscured the Se signal. Five scans were collected for Au, and all spectra were normalized to the Au $4f_{7/2}$ peak at 84.0 eV.

4.5 ζ Potential Measurements

We use a Malvern Zetasizer Nano to determine the zeta potential of QDs in water. We use a refractive index of 2.64[4] with four runs of 20 scans each, of which we discard the first run as an equilibration run for the calculations of average zeta potentials. We use the Smoluchowski model for the zeta potential calculation. The instrument is equipped with a He-Ne laser operating at 633 nm. We cannot bring the solution more basic than pH 10 for the ζ potential experiments due to the pH limitations of the electrodes in the ζ potential cell. “Basic I” refers to pH 10 for the ζ potential measurements.

5. CHARACTERIZATION

5.1 Determination of the Concentration of the QDs in Water

To determine the QD concentration in water, we used the pH 7 spectra of HCl-, PPA-, and MPA-exchanged QDs. With the HCl-and PPA-exchanged QDs, we first subtracted the exponential scattering baseline as shown in **Figure S2**. For the exponential-subtracted HCl- and PPA-exchanged QDs and for the raw MPA spectra, we then fit the first excitonic absorbance peak to a Gaussian.

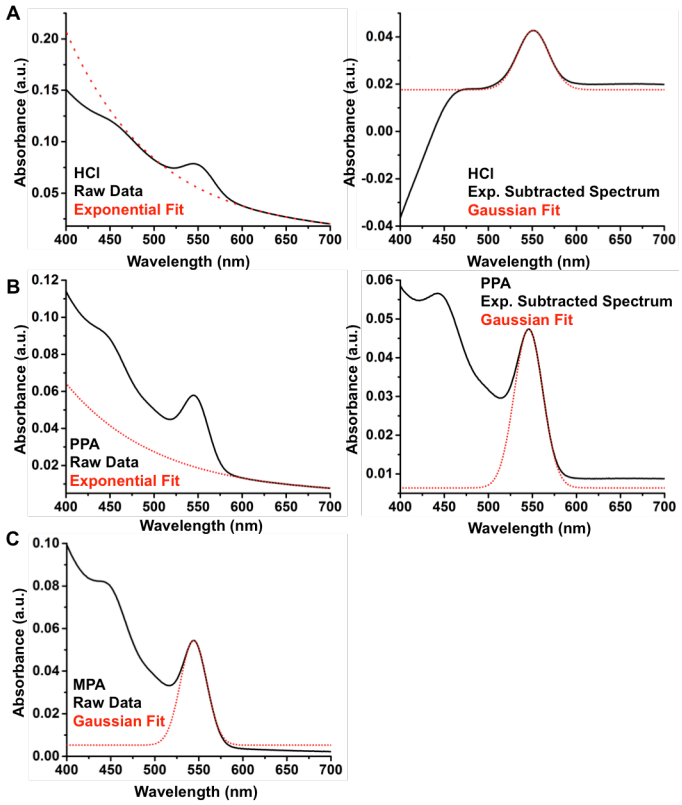

Figure S2. Representative absorbance fitting spectra for HCl- **(A)**, PPA- **(B)**, and MPA-exchanged **(C)** CdSe QDs. The samples contain 0.6 µM CdSe with 150 eq. of HCl, 0.6 µM CdSe with 300 eq. PPA, or 0.7 µM CdSe with 300 eq. MPA The concentrations of the QDs in water vary due to the differential yield of phase transfer into water as a function of the ligand used for the exchange procedure. The spectra for all three ligands are taken from the pH 5 sample.

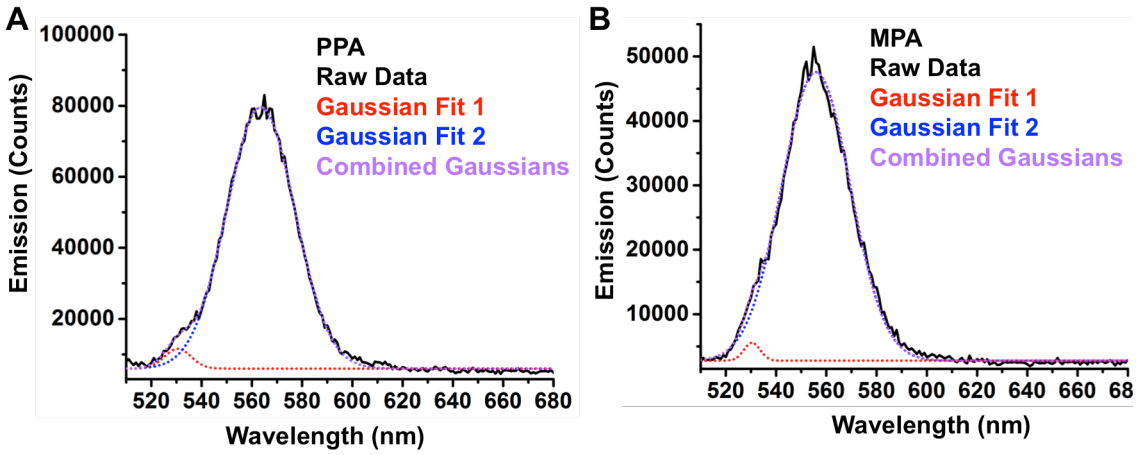

Figure S3. Representative emission fitting spectra for PPA- **(A)** and MPA-exchanged **(B)** CdSe QDs. The samples contain 0.6 µM CdSe with 300 eq. PPA or 0.7 µM CdSe with 300 eq. MPA The concentrations of the QDs in water vary due to the differential yield of phase transfer into water as a function of the ligand used for the exchange procedure. The spectra for both ligands are taken from the pH 5 sample. The small peak around 530 nm (red trace) is a Raman peak.

We fit the emission spectra, shown in **Figure S3** of PPA- and MPA-exchanged QDs to two Gaussians, one of which is a small Raman peak at 530 nm. We then used the calibration curve from Yu *et al.*[5] to determine the QD concentration. For the HCl-exchanged QDs, we were unable to measure the FWHM of the emission because these QDs are non-emissive, so we approximated using the FWHM of the PPA-exchanged QDs.

5.2 Determination of the pH of QDs in Water

For the HCl- and MPA-exchanged QDs we added one equivalent of KOH per ligand added (150 equivalents of HCl per QD and 300 equivalents of MPA per QD) during the ligand-exchange/phase-transfer procedure and expected the resulting pH of the QDs in water post-exchange to be pH ~7. Upon measurement with a pH meter (Corning Model 130), however, the resulting pH was determined to be pH ~6.

For the PPA-exchanged QDs, we added two equivalents of KOH per ligand added (300 equivalents of PPA per QD) to achieve an expected pH of 9.5 post-exchange. The measured pH of the resulting PPA/QD solution after the ligand-exchange/phase-transfer procedure, however, was measured to be ~7.5.

5.3 Quantification of Bound Ligands

For displaced oleic acid determination, we used hexamethyltrisiloxane as an internal quantification standard, with 18 equivalent protons at 0.22 ppm in C_6D_6. To determine the number of bound MPA or PPA in water we used 0.4 mM tetramethylammonium

nitrate, which has 12 equivalent protons at 3.18 ppm in 80/20 (v/v) H_2O/ D_2O. We fit the tetramethylammonium peak with a Lorentzian and fit the alkyl protons of PPA or MPA with multiple Lorentzians to determine accurate relative areas for each set of protons. From this relative integration, we obtained the number of freely diffusing (i.e., unbound) ligands in solution. We then used signal subtraction, as previously described,[6] to determine the number of ligands bound per QD. In the PPA case, the quantification of PPA in the samples with and without QDs present was identical within the sensitivity of the instrument, indicating that PPA is in rapid exchange on and off the surface of the QD on the NMR time scale.

5.4 Derivation of ^{1}H NMR Chemical Shift Fitting Equations

Figures S12A and S13A show the pH dependence of the chemical shift of the alkyl protons of PPA alpha to the phosphonic acid group. With increasing basicity of the solution, the resonances for the alkyl protons indicated in **Figure S12A** shift upfield due to the decreased shielding of the H^+ nucleus. The observed chemical shift at a given pH is a weighted average of the absolute value of the chemical shifts of each individual species of PPA, as described by **eq. S1**. In **eq. S1**,

$$\delta_{\mathrm{obs}} = \mathrm{n_{PPA}}\delta_{\mathrm{PPA}} + \mathrm{n_{PPA^-}}\delta_{\mathrm{PPA^-}} + \mathrm{n_{PPA^{2-}}}\delta_{\mathrm{PPA^{2-}}} + \mathrm{n_{PPA^{3-}}}\delta_{\mathrm{PPA^{3-}}} \quad \textbf{(S1)}$$

δ_{obs} indicates the observed chemical shift at a given pH, n indicates the mole fraction of PPA present as the indicated subscript, and δ indicates the absolute chemical shift value if all of the PPA in solution was present as the species indicated by the subscript.

The parameters $\mathrm{n_{PPA}}$, $\mathrm{n_{PPA^-}}$, $\mathrm{n_{PPA^{2-}}}$, and $\mathrm{n_{PPA^{3-}}}$ are defined by **eqs. S2-S5**, where K_1

$$\mathrm{n_{PPA}} = \frac{[\mathrm{H^+}]^3}{[\mathrm{H^+}]^3+[\mathrm{H^+}]^2\mathrm{K_1}+[\mathrm{H^+}]\mathrm{K_1K_2}+\mathrm{K_1K_2K_3}} \quad \textbf{(S2)}$$

$$\mathrm{n_{PPA^-}} = \frac{[\mathrm{H^+}]^2\mathrm{K_1}}{[\mathrm{H^+}]^3+[\mathrm{H^+}]^2\mathrm{K_1}+[\mathrm{H^+}]\mathrm{K_1K_2}+\mathrm{K_1K_2K_3}} \quad \textbf{(S3)}$$

$$\mathrm{n_{PPA^{2-}}} = \frac{[\mathrm{H^+}]\mathrm{K_1K_2}}{[\mathrm{H^+}]^3+[\mathrm{H^+}]^2\mathrm{K_1}+[\mathrm{H^+}]\mathrm{K_1K_2}+\mathrm{K_1K_2K_3}} \quad \textbf{(S4)}$$

$$\mathrm{n_{PPA^{3-}}} = \frac{\mathrm{K_1K_2K_3}}{[\mathrm{H^+}]^3+[\mathrm{H^+}]^2\mathrm{K_1}+[\mathrm{H^+}]\mathrm{K_1K_2}+\mathrm{K_1K_2K_3}} \quad \textbf{(S5)}$$

indicates the first acid dissociation constant of PPA, K_2 indicates the second acid dissociation constant, and K_3 indicates the third acid dissociation constant.

We fit the PPA only samples and the PPA with QDs samples in **Fig. S14A** with **eq. S6**,

$$\delta_{obs} = \frac{[H^+]^2K_1\delta_{PPA^-}+[H^+]K_1K_2\delta_{PPA^{2-}}+K_1K_2K_3\delta_{PPA^{3-}}}{[H^+]^3+[H^+]^2K_1+[H^+]K_1K_2+K_1K_2K_3} \quad \textbf{(S6)}$$

which accounts for the chemical shift values only of mono-, di-, and tri-deprotonated PPA, since there is no neutral PPA present over the pH range of our NMR data. From fitting both of these data sets, we obtain pK_a's of 8.22 ± 0.01 for the PPA only data set and 8.20 ± 0.04 for the data set with QDs and PPA as shown in **Fig. S13A**. Data for the other set of alkyl protons is shown in **Figure S4**. These pK_a values are in good agreement with both the pK_a obtained by acid-base titration of freely diffusing PPA, 8.0 ± 0.1, and with previously reported literature values for freely diffusing PPA.[7]

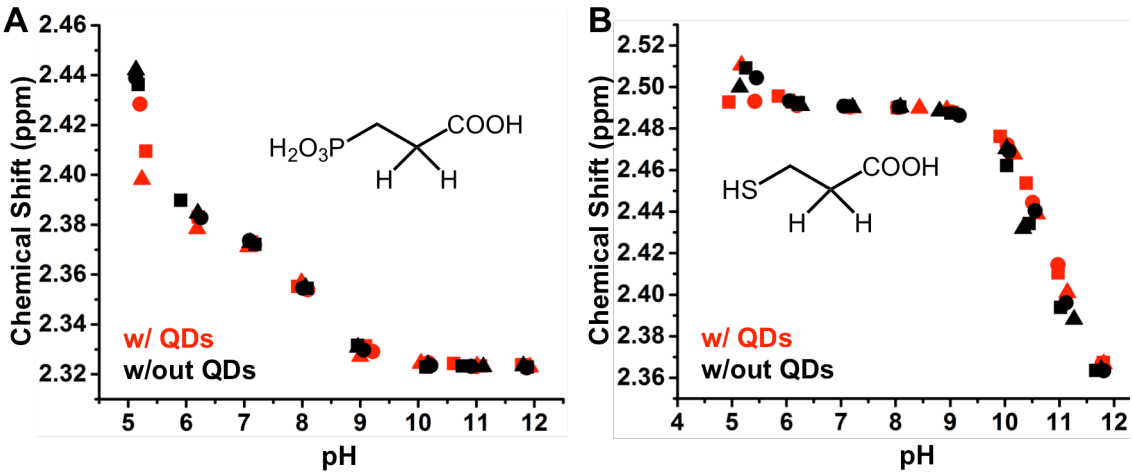

Figure S4. Plots of the chemical shift of alkyl protons nearest to the carboxylate group of PPA **(A)** or MPA **(B)** (bolded) as a function of pH with (red) and without (black) CdSe QDs in solution. The insets show the measured concentrations of PPA or MPA in the corresponding samples. Each sample contains 2 mM PPA or 1.8 mM MPA, and 0.4 mM tetramethylammonium nitrate as an integration standard in 80/20 (v/v) H_2O/ D_2O. The "w/ QDs" samples also contain 3.7 µM CdSe QDs **(A)** or 5.7 µM CdSe QDs **(B)**. The concentrations of the QDs in water vary due to the differential yield of phase transfer into water as a function of the ligand used for the exchange procedure.

We determine the thiolate pK_a for both the MPA only samples and MPA when QDs are present (**Figure S13B**) using **eq. S7**,

$$\delta_{obs} = \frac{[H^+]K_1\delta_{MPA^-} + K_1K_2\delta_{MPA^{2-}}}{[H^+]^2+[H^+]K_1+K_1K_2} \textbf{ (S7)}$$

which is derived in the same way as **eq. S6** except that we account for only two protonation equilibria with MPA.

Fitting to **eq. S7** yields pK_a's of 10.69 ± 0.05 for the MPA only data set and 10.86 ± 0.02 for the data set with QDs and MPA. Data for the other set of alkyl protons is available in **Figure S4**. We attribute this small but statistically significant deviation in the observed pK_a's to the binding equilibrium of MPA, where the pK_a determined in the case where QDs are present in solution is the "pK_a observed," not the pK_a of truly QD-bound MPA, where the pK_a observed is a weighted average of the freely diffusing MPA pK_a and the pK_a of the truly QD-bound MPA, for which we do not observe an NMR signal.

5.5 Determination of Excess Cadmium at the QD Surface

We performed inductively-coupled plasma-optical emission spectrometry to determine the Cd:Se ratio of the QDs exchanged with PPA and HCl. We calculated a Cd:Se ratio of (1.6 ± 0.1):1 for PPA-exchanged QDs and (1.7 ± 0.1):1 for HCl-exchanged QDs in water, which corresponds to about one monolayer of excess cadmium atoms at the QD surface in both cases, in agreement with previous reports.[8]

5.6 Determination of the Binding Energy of the XPS Spectra

We fit the PPA-exchanged samples equilibrated at pH 7 (Neutral I in black, **Figure 2B**) with one Gaussian and fit the samples equilibrated at pH 12 (Basic I in red, **Figure 2B**) with two Gaussians, one of which was fixed at the peak position of Neutral I. We fit the PPA-exchanged samples equilibrated at pH 7 after equilibration at pH 12 (Neutral II in blue, **Figure 2B**) to two Gaussians, one of which was fixed at the peak position of Basic I. **Table S1** shows the average binding energies for all samples in **Figure 2B** in the main text.

Table S1. The $Cd_{5/2}$ and $Cd_{3/2}$ Binding Energies for the data shown in Figure 2B

	$Cd_{5/2}$ Binding Energy (eV)	$Cd_{3/2}$ Binding Energy (eV)
CdO	412.25 ± 0.06	405.51 ± 0.06
CdSe-OA	412.0969 ± 0.0009	405.361 ± 0.001
γ-$Cd(OH)_2$	411.390 ± 0.005	404.634 ± 0.005
pH 7	411.3 ± 0.4	404.6 ± 0.4
pH 12[a]	412.68 ± 0.09	405.94 ± 0.09
pH 12 to 7	411.5 ± 0.3[b]	405.94 ± 0.09[b]
	411.1 ± 0.4[c]	404.5 ± 0.3[c]

[a]The reported data is for the population of cadmium with a higher binding energy. The data for the population of cadmium with a lower binding energy in these samples is fixed to the values for the pH 7 sample.
[b]The population of cadmium with a higher binding energy.
[c]The population of cadmium with a lower binding energy.

6. DETAILS OF THE THEORETICAL MODEL

6.1 Theoretical Approach

In this section we set out to develop a theoretical model to describe the charging of a QD due to the adsorption of PPA. The dual objective of the theoretical model is to gain insights into the effect that pH and other solution conditions have on PPA adsorption and the charge of the QD and relate this to the experimental findings. Previously, coarse-grained molecular dynamics (MD) simulations have been performed to estimate the binding constant of ligands to CdSe QDs.[9] Such simulation approaches, although they include molecular details, do not generally include the possibility of protonation-deprotonation of the ligand in solution and adsorbed on the QD. Here we employ a generalized Poisson-Boltzmann approach that includes the possibility of (de)protonation of the ligand. This approach is based on the one previously developed to describe thermodynamic and structural properties of end-tethered weak polyelectrolytes, i.e., polyelectrolytes whose degree of charge is not fixed but can change depending on

environmental conditions, like pH.[10] Particularly relevant are the predictions of the charged state of acid-ligated gold nanoparticles, which were in good agreement with experimental observations.[11] Likewise, we used a similar approach to investigate the effect of solution conditions on the charge regulation of bacteriophage capsids.[12]

6.2 Free Energy Functional

We consider a QD of radius R that is in contact with an aqueous solution containing PPA ligands at a concentration c_{PPA}. The reservoir is characterized by a given pH and contains either monovalent TBCl (tetrabutylammonium chloride) salt or $TMNO_3$ (tetramethyl-ammonium nitrate) salt. The pH is adjusted by adding KCl or HNO_3 as appropriate. The PPA ligand has five (de)protonation states associated with the phosphate and the carboxylic groups of the ligand. They are denoted as follows $AH_2BH, AH^-BH, AH^-B^-, A^{2-}BH$, and $A^{2-}B^-$, with BH referring to the carboxylic group and AH_2 denoting the phosphonate group. The acid-base reactions are

$$AH_2BH \rightleftarrows AH^-BH + H^+, \quad \textbf{(S8)}$$
$$AH^-BH \rightleftarrows AH^-B^- + H^+, \quad \textbf{(S9)}$$
$$AH^-BH \rightleftarrows A^{2-}BH + H^+, \quad \textbf{(S10)}$$
$$AH^-B^- \rightleftarrows A^{2-}B^- + H^+. \quad \textbf{(S11)}$$

We assume that the QD has N adsorption sites for the ligand PPA. The resulting number of adsorption or binding sites per unit area is then $\sigma = N_s/A(R)$. Here, $A(R)$ is the surface area of the QD.

The free energy of a QD with adsorbed chargeable ligands is composed of contributions stemming from the acid-base chemical equilibrium of the PPA ligands, the entropy of the mobile ions and ligands, the electrostatic interaction energy, a free energy contribution related to adsorption and electrostatic energy of the adsorbed PPA ligands, and a free energy contribution related to counterion condensation, specifically:

$$F = -TS_{mix} + F_{chem} + F_{elect} + E_{rep} + F_{surf}. \quad \textbf{(S12)}$$

The first term in the free energy corresponds to the mixing or translational entropy of mobile ionic species

$$-\frac{S_{mix}}{k_B T A(R)} = \sum_k \int dr\, G(r)\, \rho_k(r)(\ln \rho_k(r)\, v_w - 1), \quad \textbf{(S13)}$$

where the index k runs over all of the different types of mobile species: the water molecule, the cations (TBA^+, TM^+, K^+), anions (NO_3^-, Cl^-), protons (H^+), hydroxide ions (OH^-), and the PPA ligands found in its five (de)protonation states $AH_2BH, AH^-BH, AH^-B^-, A^{2-}BH$, and $A^{2-}B^-$. The variable $\rho_k(r)$ corresponds to the number density of mobile species k, and v_w is the volume of a water molecule, which is used as the unit of volume. Note that the QD is in contact with an aqueous solution of given pH containing monovalent $TMNO_3$ or TBCl salt, which is assumed to be completely dissociated. Note that we employed spherical coordinates to reflect the symmetry of the QD, and assumed the system to be laterally homogeneous and only explicitly anisotropic in the radial direction *r*. Here the function $G(r)$ is the Jacobian determinant divided by the area of the NP: $G(r) = A(r)/(R)$ and equals $(r/R)^2$. [13]

The second term in the free energy describes the chemical free energy of the ligand molecules in solution:

$$\frac{\beta F_{chem}}{A(R)} = \sum_i \beta\mu_i^0 \int dr\ G(r)\ \rho_i(r). \quad \textbf{(S14)}$$

Here, i runs over the different protonation states of the PPA ligand as well as the proton and hydroxide ions, and μ_i^0 corresponds to the standard chemical potential molecule i.

The third term in the free energy functional describes the electrostatic contribution to the free energy [14] and is given by

$$\frac{\beta F_{elect}}{A(R)} = \beta \int dr\ G(r) \left[\langle\rho_q(r)\rangle\psi(r) - \frac{1}{2}\epsilon_0\epsilon_w\left(\nabla_r\psi(r)\right)^2\right]. \quad \textbf{(S15)}$$

Here, $\psi(r)$is the electrostatic potential and $\langle\rho_q(r)\rangle$ is the total charge number density. In the above functional ϵ_0 and ϵ_w correspond to the dielectric permittivity of vacuum and the relative dielectric constant of the aqueous solution respectively, the latter having a value of $\epsilon_w = 78.5$. The total charge number density is the sum of the charge number density of all charged species:

$$\langle\rho_q(r)\rangle = \sum_i e\ z_i\ \rho_i(r). \quad \textbf{(S16)}$$

Here, the summation runs over all charged mobile ions ($\mathrm{TBA^+}, \mathrm{TM^+}, \mathrm{K^+}, \mathrm{NO_3^-}, \mathrm{Cl^-}, \mathrm{H^+}, \mathrm{OH^-}$), and the charged ligand molecules $\mathrm{AH^-BH}, \mathrm{AH^-B^-}, \mathrm{A^{2-}BH}, \text{and } \mathrm{A^{2-}B^-}$ where z_i is their valence and e is the unit of charge.

The repulsive interactions in the theory are modeled as excluded volume interactions. The intermolecular excluded volume interactions are accounted for by assuming that the system is incompressible at every position:

$$\sum_k \phi_k(r) = 1. \quad \textbf{(S17)}$$

Here, $\phi_k(r) = \rho_k(r)v_k$, the volume fraction of species k with v_k corresponding to its volume. These volume constraints are enforced through the introduction of Lagrange multipliers, $\pi(r)$. Formally, they are not part of the Helmholtz free energy, since they are added as a constraint.

The last term, F_{surf}, describes the surface free energy contribution to the free energy and is equal to

$$\frac{\beta F_{surf}}{A(R)} = \beta\sigma_q\psi(R) + \sigma_R\left(\ln\frac{\sigma_R}{\sigma} + \beta\mu_R^0\right) + \sum_i \sigma_{LR,i}\left(\ln\frac{\sigma_{LR,i}}{\sigma} + \beta\mu_{LR,i}^0\right) + \sum_k \sigma_{RM,k}\left(\ln\frac{\sigma_{MR,k}}{\sigma} + \beta\mu_{RM,k}^0\right). \quad \textbf{(S18)}$$

Here, the first contribution describes the electrostatic surface free energy arising for the surface charge on the QD, with σ_q corresponding to the total surface charge density. The second term corresponds to the free energy of mixing of binding sites that are unbound, i.e., have no adsorbed PPA ligands or condensed counterions, and the third term describes the standard free energy associated with the free binding site. The last four terms, similarly, describe the free energy of mixing and standard chemical potential associated with the adsorbed PPA ligands (LR, i) and condensed counterions (MR, k). The areal density or surface coverage of the free sites is denoted as σ_R, while the

adsorbed ligand surface coverages are denoted by $\sigma_{LR,i}$ and $\sigma_{RM,k}$ corresponds to the area density of the adsorbed counterions. The index i corresponds to the different charged states of the PPA ligand, while k runs over the different types of counterions. Consequently, the total surface charge density of the QD is the sum of the charges from the adsorbed ligands and the charge of the free, unbound 'receptor' site.

$$\sigma_q = \sum_i \sigma_{LR,i} z_{LR,i}\, e + \sigma_R z_R\, e. \quad \textbf{(S19)}$$

Here $z_{LR,i}$ corresponds to the valence of the absorbed PPA ligand and z_R is the valence of the free binding site, which we set to +1 (effective surface charge of undercoordinated Cd^{2+}). We assume that PPA binds to the QD with the '"first" deprotonated oxygen group of the phosphate group and neutralizes the opposing surface charge. Other binding mechanisms, like the binding of the deprotonated carboxylic acid or the charged secondary and tertiary oxygen of the phosphonate group are not considered as they are assumed to be too weak to substantially contribute to ligand adsorption. Thus, we assume that the neutral PPA does not bind to the surface. Likewise, we do not consider binding of the carboxylic group of the PPA with the surface. This implies the occurrence following surface acid-base equilibrium reactions

$$> \mathrm{RAHBH} \;\rightleftarrows\; > \mathrm{RAHB^-} + \mathrm{H^+}, \quad \textbf{(S20)}$$
$$> \mathrm{RAHBH} \;\rightleftarrows\; > \mathrm{RA^-BH} + \mathrm{H^+}, \quad \textbf{(S21)}$$
$$> \mathrm{RAHB^-} \;\rightleftarrows\; > \mathrm{RA^-B^-} + \mathrm{H^+}. \quad \textbf{(S22)}$$

Finally, the counterion condensation of the negatively charged ions $\mathrm{OH^-}$, $\mathrm{NO_3{}^-}$, and $\mathrm{Cl^-}$ is included along similar lines as the acid-base chemical reaction of the ligands:

$$> \mathrm{R^+} + \mathrm{OH^-} \rightleftarrows > \mathrm{ROH}, \quad \textbf{(S23)}$$
$$> \mathrm{R^+} + \mathrm{NO_3^-} \;\rightleftarrows\; > \mathrm{RNO_3}, \quad \textbf{(S24)}$$
$$> \mathrm{R^+} + \mathrm{Cl^-} \;\rightleftarrows\; > \mathrm{RCl}. \quad \textbf{(S25)}$$

The sum of the free binding sites and the adsorbed ligand and counterion condensed sites is equal to the total number of adsorption sites:

$$\sigma_R + \sum_i \sigma_{LR,i} + \sum_k \sigma_{RM,k} = \sigma. \quad \textbf{(S26)}$$

The total free energy is minimized with respect to $\rho_i(r)$, σ_R, $\sigma_{LR,i}$ and $\$\sigma_{RM,k}$, and varied with respect to the electrostatic potential, $\psi(r)$, under the constraints of incompressibility and the fact that the system is in contact with a bath of cations, anions, protons, hydroxide ions, and PPA ligands. Therefore the proper thermodynamic potential is the semi-grand potential,[15, 16] which is given by

$$\frac{\beta W}{A(R)} = \sum_l \int dr\, G(r)\, \rho_l(r)(\ln \rho_l(r)\, v_w - 1 + \beta\mu_l^0)$$
$$+ \beta \int dr\, G(r) \left[\langle \rho_q(r)\rangle \psi(r) - \frac{1}{2}\epsilon_0\epsilon_w \left(\nabla_r \psi(r)\right)^2\right] + \beta\sigma_q\psi(R)$$
$$+ \sigma_R \left(\ln \frac{\sigma_R}{\sigma} + \beta\mu_R^0\right) + \sum_i \sigma_{LR,i} \left(\ln \frac{\sigma_{LR,i}}{\sigma} + \beta\mu_{LR,i}^0\right)$$
$$+ \sum_k \sigma_{RM,k} \left(\ln \frac{\sigma_{MR,k}}{\sigma} + \beta\mu_{RM,k}^0\right) + \beta \int dr\, G(r)\, \pi(r) \left(\sum_l \rho_l(r) v_l - 1\right)$$
$$+ \beta\lambda \left(\sigma_R + \sum_i \sigma_{LR,i} + \sum_k \sigma_{RM,k} - \sigma\right)$$
$$- \sum_{j=\{\mathrm{TBA^+,TM^+,K^+}\}} \beta\mu_j \int dr\, G(r)\ \rho_j(r)$$
$$- \sum_i \beta\mu_{L,i} \left(\left[\int dr\, G(r)\ \rho_{L,i}(r)\right] + \sigma_{LR,i}\right)$$
$$- \sum_{i=\{\mathrm{OH^-,NO_3^-,Cl^-}\}} \beta\mu_{M,i} \left(\left[\int dr\, G(r)\ \rho_i(r)\right] + \sigma_{MR,i}\right)$$
$$- \mu_{H^+} \left(\int dr\, G(r) \left[\rho_{H^+}(r) + \sum_m (3 + z_{L,m})\rho_{L,m}(r)\right]\right.$$
$$\left. + \sum_i (2 + z_{LR,i})\sigma_{LR,i}\right). \quad \textbf{(S27)}$$

Here $\mu_\gamma$is the chemical potential of molecules of type γ. Note that since we assume that the adsorbed PPA ligands are in thermodynamic equilibrium with the PPA molecules in solution, their chemical potentials are identical: i.e., $\mu_{L,i} = \mu_{LR,i}$. Similarly, $\mu_{M,k} = \mu_{MR,k}$ holds. The last integral accounts for the total number of protons in the system, which is the sum of the free protons and those that are in the protonated states of the free and adsorbed PPA ligands.

The above presented free energy functional corresponds to a generalized Poisson-Boltzmann approach. Common Poisson Boltzmann approaches only involve the translational entropy of the ions and electrostatic interactions, as described by the first line. The subsequent terms in the free energy, usually not considered, describe the adsorption and charge regulation of the ligands and the excluded volume repulsions within the electrolyte solution.

Minimization of the free energy yields the following expression for the local volume fraction of the solvent

$$\phi_w(r) = \rho_w(r) v_w = e^{-\beta\pi(r)v_w}, \qquad \textbf{(S28)}$$

while the density of the ions is

$$\rho_k(r) = \frac{1}{v_w} e^{-\beta(\mu_k^0 - \mu_k)} e^{-\beta\pi(r)v_k} e^{-\beta\psi(r)z_k e}. \quad \textbf{(S29)}$$

It is important to point out that the chemical potential of water does not need to be specified explicitly because the incompressibility constraint reduces the number of thermodynamically independent variables. Therefore, the chemical potentials, μ_k, are, in reality, exchange chemical potentials, which correspond to the difference between the chemical potential of the species k and that of water. Likewise, the charge neutrality, the water self-dissociation equilibrium, and the acid-base equilibrium of the PPA ligand further reduce the number of thermodynamic independent variables. The values of the exchange chemical potential of the remaining species can be expressed by relating them to their bulk or reservoir concentrations:

$$\rho_k^{bulk} v_w = e^{-\beta(\mu_k^0 - \mu_k)} e^{-\beta \pi^{bulk} v_k} e^{-\beta \psi^{bulk} z_k e}, \qquad \textbf{(S30)}$$

with $\psi^{bulk} = 0$, see below in **Eq. (S.32)**. Further discussions of this aspect of the theory can be found in e.g., Refs 9 and 14.[10, 15] The bulk concentrations of the different states of the ligands are dependent on the overall ligand concentration, c_{PPA}, pH, and their chemical equilibrium constants as explained below.

Here, we briefly outline how we can obtain the bulk concentrations for the different protonation states of the ligand. Consider, e.g. the reaction $\mathrm{AH_2BH} \rightleftarrows \mathrm{AH^-BH} + \mathrm{H^+}$. Combining the expressions for the number densities of $\mathrm{AH_2BH}, \mathrm{AH^-BH}$ and $\mathrm{H^+}$ yields following reaction equation:

$$\frac{\rho_{\mathrm{AH^-BH}}(r)\rho_{\mathrm{H^+}}(r)}{\rho_{\mathrm{AH_2BH}}(r)} = \frac{1}{v_w} K_a^0 e^{-\beta \pi(r) \Delta v_a}. \quad \textbf{(S31)}$$

Here, the variable $K_a^0 = e^{-\beta \Delta G_a^0}$ corresponds to the chemical equilibrium and ΔG_a^0 is the standard free energy change of the reaction and Δv_a is the volume change of the reaction. The chemical equilibrium constant K_a^0 is related to the experimental equilibrium constant $K_a = C\, e^{-\beta \Delta G_a^0}$ of a single acidic molecule in infinitely dilute solution. Here *C* is a constant required for consistency of units and equal to $C = 1/N_A v_w$ where N_A is Avogadro's number. For the reaction: $\mathrm{AH_2BH} \rightleftarrows \mathrm{AH^-BH} + \mathrm{H^+}$, the standard free energy change is given as $\Delta G_a^0 = \mu^0_{\mathrm{AH^-BH}} + \mu^0_{\mathrm{H^+}} - \mu^0_{\mathrm{AH_2BH}}$ while the change in volume is equal to $\Delta v_a = v_{\mathrm{AH^-BH}} + v_{\mathrm{H^+}} - v_{\mathrm{AH_2BH}}$. We can write down similar equations for the other acid-base reactions. The result is a set of equations for the concentrations of the different protonation states of the PPA ligand, $\rho_{L,i}^{bulk}$, which can readily be solved numerically, under the assumption of incompressibility, charge neutrality, and mass balance for a given bulk or reservoir ligand concentration, c_{PPA}, pH, and salt concentration. The required $\mathrm{pK_a}$ values are listed in **Table S2** and Ref. 16.[17]

Functional variation of the free energy with respect to the electrostatic potential yields the Poisson equation and its boundary conditions:

$$-\epsilon_0 \epsilon_w \nabla_r^2 \psi(r) = \langle \rho_q(r) \rangle \text{ and } -\epsilon_0 \epsilon_w \left. \frac{d\psi(r)}{dr} \right|_{r=R} = \sigma_q \text{ and } \lim_{r \to \infty} \psi(r) = 0. \quad \textbf{(S32)}$$

Minimization of the free energy with respect to the number free binding sites, σ_R, the amount of adsorbed PPA sites, $\sigma_{LR,i}$, and the number of condensed counterions, $\sigma_{MR,k}$: $\delta W/\delta \sigma_R = 0$, $\delta W/\delta \sigma_{LR,i} = 0$ and $\delta W/\delta \sigma_{MR,k} = 0$ results in following adsorption isotherm:

$$\sigma_R = \frac{\sigma}{q} \text{ and } \sigma_{LR,i} = \sigma_R\, q_{LR,i} \text{ and } \sigma_{LR,i} = \sigma_R\, q_{LR,i}, \quad \textbf{(S33)}$$

where

$$q = 1 + \sum_i q_{LR,i} + \sum_k q_{MR,k} \text{ , (S.34)}$$

$$q_{LR,i} = \exp\left(-\beta\left(z_{LR,i} - z_R\right)e\psi(R)\right)\exp(-\beta\Delta G_i^0)\exp\left(-\beta\left(\mu_{L,i}^0 - \mu_{L.i}\right)\right)\exp\left(-\beta\mu_{\mathrm{H}^+}\left(2 + z_{LR,i}\right)\right), \quad \textbf{(S35)}$$

$$q_{MR,k} = \exp\left(-\beta\left(z_{MR,k} - z_R\right)e\psi(R)\right)\exp(-\beta\Delta G_k^0)\exp\left(-\beta\left(\mu_{MR,k}^0 - \mu_{MR.k}\right)\right). \quad \textbf{(S36)}$$

Here $q_{LR,i}$ is the Boltzmann factor of the adsorbed PPA ligand in protonation state i and $q_{MR,k}$ corresponds to the Boltzmann factor of the condensed counterions. Strictly speaking, both $q_{LR,i}$ and $q_{MR,k}$ describe the Boltzmann factor of the adsorbed PPA ligand and condensed counterion relative to the Boltzmann factor of the free binding site. Thus, q is proportional to the partition function of a single QD. Using the free energy of the free binding site as reference energy, q becomes equal to the partition function of the QD. In the above expression, $\Delta G_i^0 = \mu_{\mathrm{LR,i}}^0 + \mu_{\mathrm{R}}^0 - \mu_{\mathrm{L,i}}^0$, corresponds to the free energy change of the adsorption of PPA ligands in protonation state i. Here ΔG_k^0 is the free energy change related to counterion condensation of counterion k. It is defined in a completed analogous way as the free energy of ligand adsorption. This binding or adsorption free energy can be written in terms of a chemical equilibrium constant, K_i^0, which is related via

$$K_i^0 = e^{-\beta\Delta G_i^0} = N_A v_w K_{ads}, \textbf{(S37)}$$

to experimentally measurable adsorption chemical constants, where N_A is Avogadro's number (note the reference state concentration is chosen to be 1 M). Finally, from **Eq. S33** it follows that the fraction of adsorbed PPA ligands in state i, $f_{LR,i}$ is defined as

$$f_{LR,i} = \frac{q_{LR,i}}{\sum_j q_j} = \frac{q_{LR,i}}{q-1}. \quad \textbf{(S38)}$$

The isotherm can be considered to be a generalized Langmuir-Davis isotherm. [18-20] Using **Eqs. S.28**, **S.37**, and **S.30**, we write $q_{LR,i}$ as

$$q_{LR,i} = \exp\left(-\beta\left(z_{LR,i} - z_R\right)e\psi(R)\right)K_i^0\ \frac{\rho_{L,i}^{bulk} v_w}{(\rho_w^{bulk} v_w)^{v_{l,i}/v_w}}. \quad \textbf{(S39)}$$

This expression shows that the isotherm or amount of adsorption depends directly on the bulk ligand concentrations, the chemical (adsorption) constants, K_i^0 and the electrostatic surface potential, $\psi(R)$ and indirectly on the acid-base equilibrium of the ligands and the electrostatic interactions due to the pH and salt concentration.

To obtain the adsorption isotherm we need to solve the Poisson Equation and incompressibility constraint, since the unknowns in **Eq. S28**, **Eq. S29**, and **Eqs. S33-S36** are the Lagrange multipliers or lateral pressures, $\pi(r)$, and the electrostatic potential, $\psi(r)$. The amount of adsorbed ligands, their protonation states, and the number of free binding sites, as well as the number of sites condensed with counterions, the density of the ions, the solvent and ligands in solution, are known once the lateral pressures and the electrostatic potential are known. Solutions for these variables can be obtained numerically, with the following procedure. Expressions of the volume fractions of all components are substituted into the incompressibility constraint

Eq. (S.17) and the Poisson equation. **Eq. (S.32)** This results in a set of non-linear integro-differential equations whose solution will determine the lateral pressure and the electrostatic potential. By discretizing space, the differential equations are converted into a set of coupled non-linear algebraic equations that can be solved by standard numerical techniques. [21] Details on the discretization procedure and numerical methods can be found in Refs. 11 and 14.[12, 15] The inputs required to solve the non-linear equations are the ligand concentration, c_{PPA}, pH, the salt concentrations of KCl and $TMNO_3$ or TBCl the volume of all species listed in **Table S3**, the surface density or number of adsorption sites, σ, on the QD, the radius of the QD, and the acid-base equilibrium constants (pK_as) of the different protonation states, listed in **Table S2**, and the binding constants of the ligand and counterions with the QD surface.

Table S2. Acid base chemical equilibrium constants for PPA[17]

reaction	pK_a
$AH_2BH \rightleftarrows AH^-BH + H^+$	2.26
$AH^-BH \rightleftarrows AH^-B^- + H^+$	4.6
$AH^-BH \rightleftarrows A^{2-}BH + H^+$	5.4
$AH^-B^- \rightleftarrows A^{2-}B^- + H^+$	6.9

Table S3. Volumes

	w	ppa	H^+	OH^-	K^+	TM^+	NO_3^-	TB^+	Cl^-
$v(nm^3)$	0.03	0.0792	0.03	0.03	0.011	0.523	0.113	0.523	0.0248

6.3 SUPPLEMENTARY FIGURES FROM THEORY

In the following section we will present a number of representative results of the theory: i.e., the charging behavior of the QD as a function of pH. Here, we will restrict ourselves to experimentally relevant conditions. Thus, we take the PPA ligand concentration to be $2\,\mathrm{mM}$, the salt concentration to be $c_{TMNO_3} = 0.4\,\mathrm{mM}$ and the radius of the QD to be $R = 1.45\,\mathrm{nm}$. Next, we need to determine the value of the number of binding sites, σ. The number of bound oleates to these QDs in an organic solvent is determined by NMR to be, on average, 279 oleates/QD. Assuming that the number of bound oleates is identical to the number of binding sites, we would have an upper bound for the binding site density of $\sigma = 10.5\,\mathrm{nm}^{-2}$. Upon ligand exchange and transfer of the QD to the water phase, it is found that the number of potential binding sites is reduced, based on an estimation of the number of hydroxides in solution. Irreversible chemical reactions cause a number of potential binding sites to be passivated. Based on the number of hydroxides in solution, the reduction is estimated to be 10 - 20%, yielding an upper bound for the density of binding sites of $\sigma = 8\,nm^{-2}$. Considering the observed hysteresis in the spectroscopy data (see main text) that suggests the occurrence of irreversible chemical reactions at the surface and passivation of binding sites, we considered the surface density as a 'quasi' adjustable parameter and varied the density of the binding sites and investigated the effect on the charge of the

QD. Explicitly, we consider $\sigma = 1\ \mathrm{nm}^{-2}$, $\sigma = 5\ \mathrm{nm}^{-2}$, and $\sigma = 8\ \mathrm{nm}^{-2}$, corresponding to a low, intermediate and high estimate of the density of binding sites. When converting the number of binding sites to surface density, we assumed the binding sites to all be located within the same plane, as inherent to the assumption of spherical symmetry. This assumption is only approximate.

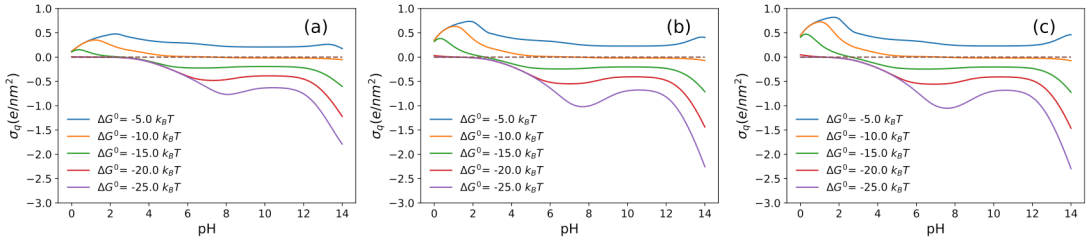

Figure S5. Total surface charge density as a function of pH for increasing binding free energy of PPA for a density of binding sites of **(a)** $\sigma = 1\ \mathrm{nm}^{-2}$, **(b)** $\sigma = 5\ \mathrm{nm}^{-2}$, and **(c)** $\sigma = 8\ \mathrm{nm}^{-2}$. The binding free energy of OH^- and NO_3^- is set to be -5 k_BT. The ligand concentration $c_{PPA} = 2\ \mathrm{mM}$ and the salt concentration equals $c_{TMNO_3} = 0.4\ \mathrm{mM}$. The QD has a radius of $R = 1.45\ \mathrm{nm}$.

Figure S5 shows the total surface charge density of the QD as a function of pH. The different lines correspond to different binding free energies, respectively from to top to bottom: -5, -10, -15, -20, and -25 k_BT. The important features are 1) the surface density is positive for weak PPA binding, 2) for sufficiently strong PPA binding free energies the surface charge density is negative and strongly dependent on the pH value of the solution, and 3) The surface charge density for the intermediate (case b) and high (case c) binding site density is almost identical. A fourth interesting observation is that the value of the total charge density of all cases considered is much smaller than the maximum feasible surface charge density. Assuming that for large binding free energies of the PPA all binding sites would be bound with PPA ligands and that for high pH values both the carboxylic and second phosphate group would be deprotonated, the total surface charge density would be equal to twice the binding density: $\sigma_q = -2\ \mathrm{e\ nm}^{-2}$, $\sigma_q = -10\ \mathrm{e\ nm}^{-2}$ and $\sigma_q = -16\ \mathrm{e\ nm}^{-2}$ respectively for case a, b, and c. Instead we find that the surface charge density for pH = 14 and $\Delta G^0 = -25\ k_BT$ equals $\sigma_q = -1.79\ \mathrm{e\ nm}^{-2}$, $\sigma_q = -2.26\ \mathrm{e\ nm}^{-2}$ and $\sigma_q = -2.30\ \mathrm{e\ nm}^{-2}$. Only for the low binding density is the surface charge density close to its maximum of $-2\ \mathrm{e\ nm}^{-2}$. Increasing the binding free energy to $-30\ k_BT$ results in $\sigma_q = -1.995\ \mathrm{e\ nm}^{-2}$. For the intermediate and high binding density, the surface charge density is far less than the expected $\sigma_q = -10\ \mathrm{e\ nm}^{-2}$ or $\sigma_q = -16\ \mathrm{e\ nm}^{-2}$ and saturates. This is because the charge of the QD does not follow the above simple picture. It arises as a complicated balance between various opposing forces that involve electrostatic repulsions, counterion and ligand confinement, and counterion ion condensation and ligand binding and the charge regulation of adsorbed ligands, i.e., shifting the equilibrium distribution of the acid-base chemical equilibria toward the less charged states.

For low PPA binding free energies insufficient ligands are adsorbed to the QD to completely neutralize all positively charged sites on the QD and hence the QD remains positively charged. The majority of binding sites are then neutralized through condensation of counterions, either OH^- or NO_3^- ions. At low pH and with increasing binding free energy more singly deprotonated PPA ligands (AH-BH) bind to the QD and the surface charged is reduced. Upon increasing pH, the carboxylic group and also the second phosphate group of the PPA are deprotonated and the QD acquires a negative charge. As further deprotonation of the absorbed ligands occurs with increasing pH, electrostatic repulsions increase between the adsorbed ligands. The QD system mitigates these electrostatic repulsions through a number of mechanisms. The first mechanism involves desorbing the absorbed charged ligands from the QD and exchanging them with PPA ligands in different less charged states. E.g., replacement of adsorbed ligands in the charged >RAHB- state with the neutral >RAHB state. Thereby reducing the number of negative charges on the QD surface. **Figure S6** demonstrates this mechanism. It presents the fraction of binding sites that are bound with ligands as a function of pH for various binding free energies. A second mechanism involves charge regulation of the absorbed PPA ligands wherein the absorbed ligand shifts their acid-base equilibrium or charged states to the less charged protonation states. This reduces the electrostatic repulsion but occurs at the cost of chemical free energies (ΔG_a^0's) of the acid-base equilibria.

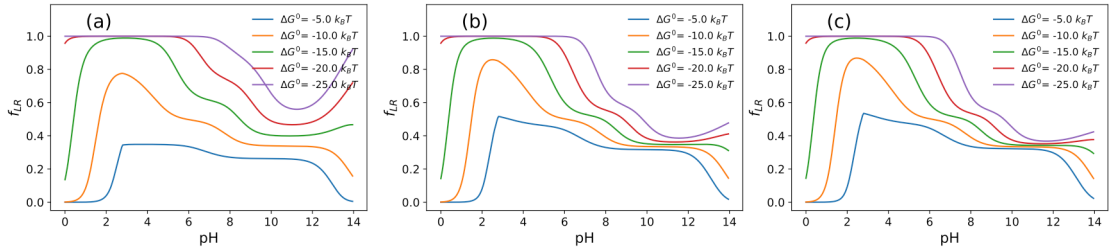

Figure S6. The fraction of binding sites that are bound with ligands as a function of pH for various binding free energies. **(a)** $\sigma = 1\ \mathrm{nm}^{-2}$, **(b)** $\sigma = 5\ \mathrm{nm}^{-2}$, and **(c)** $\sigma = 8\ \mathrm{nm}^{-2}$. The conditions are identical to **Figure S5**.

Consequently, the distribution of the fraction of binding sites that are bound with ligands varies as a function of pH for various binding free energies. Only moderate binding free energy and pH values close to the isoelectric point (both characterized by a low net charge and a low amount of electrostatic interactions) result in a distribution of charged PPA ligands similar to that of the molecule in solution. A more detailed description of charge regulation, in the context of ligated nanoparticles, can be found in Ref 10. [11]

Figure S7 illustrates the effect of charge regulation. **Figure S7a** shows the distribution of states (free, ligand adsorbed and condensed counterions) as a function of pH for $\Delta G^0 = -20\,k_BT$. For example at pH=8 a fraction of 0.46 of all binding sites are occupied by PPA ligand in $>RAHB^-$ state, which is the singly deprotonated state of the carboxylic group, and a fraction of 0.45 of the binding sites are free. The remaining binding sites are mostly bound with ligands in $>RA^-BH$ state (0.07). Increasing the pH changes the distribution drastically such that most binding sites (60%) are unoccupied, whilst the largest fraction of bound ligands are in the $>RA^-B^-$ state (31%). **Figure S7b** shows the fraction of adsorbed ligand in state $>RAHB^-$ as a function of pH. The maximum number of adsorbed ligands in the $>RAHB^-$ state shifts to higher pH values with increasing binding free energy, due in part due to the charge regulation mechanism as described above.

Finally, **Figure S7c** compares the distribution of the adsorbed ligands in their four different adsorbed states as a function of pH to the distribution of the adsorbed ligands states that would be identical to the distribution of ligands in the reservoir. The distribution of charged states of ligands in the reservoir follows the ideal solution behavior of acids in dilute solution. For the given binding free energy and binding site density, we see that the 'titration' curves are shifted by more than 2 pH units.

The results of **Figures S5-S7** provided us with an understanding of the basics phenomena that control the number of adsorbed ligands and resulting charge on the QD as a function of pH. Here we shall combine above theoretical insight with experimental observations and obtain a lower as well as an upper bound for the binding free energy of the PPA ligand, which provides insight into the strength of PPA adsorption.

Lower bound of binding free energy. **Figure S5** demonstrates that for a

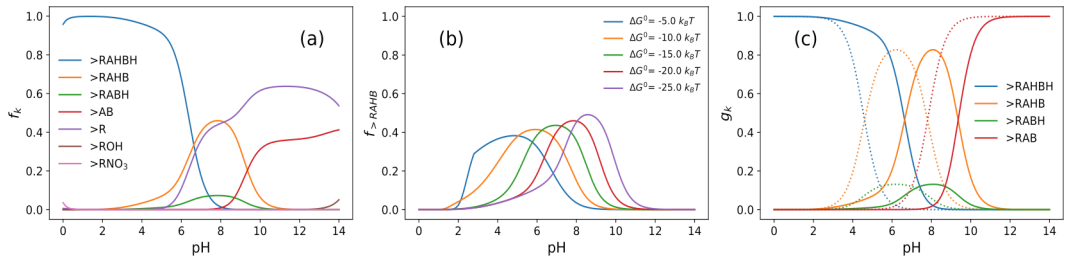

Figure S7. a) The distribution of states as a function of pH for a binding free energy $\Delta G^0_{\square} = -20\,k_BT$ and density of binding sites $\sigma = 5\,nm^{-2}$. **(b)** The fraction of adsorbed ligand in state $>RAHB^-$ as a function of pH for various binding free energies. **(c)** The fraction of ligands in their four different charged, adsorbed states as function pH for a binding free energy $\Delta G^0_{\square} = -20\,k_BT$ and density of sites $\sigma = 5\,nm^{-2}$. The dotted lines correspond to the distribution of the ligand (un)charged states in dilute solution. The fraction g_k in figure **(c)** is different from the fraction f_k. The former corresponds to the ratio of adsorbed ligand in state k, while the latter is the ratio between the number of adsorbed ligands in state k over the total amount of adsorbed ligand. ($g_k = \sigma_{LR,k}/\sum_j \sigma_{LR,j}$). The remaining conditions are identical to those for **Figure S5**.

sufficiently low binding free energy of the ligands the QDs are positively charged and that only for sufficiently large ligand binding free energies do the QDs become negatively charged. The ζ potential measurements indicate that the QD carries an effective negative charge at the slipping plane. Similarly when the pH of the solution is lower than ~5 the QDs lose their colloidal stability and the QDs start to aggregate. This is indicative of approaching the isoelectric point: the pH for which the QD does not carry a net charge. Combining these observations implies a lower bound for the binding constant of the ligands, which is estimated to be $\mathrm{K}_b \geq 400\ \mathrm{M}^{-1}$ ($\Delta G^0 \leq -10 k_B T$).

Upper bound of binding free energy. Figure S7 shows that the distribution of the differently charged states of the ligands that are adsorbed onto the QD has a distribution that is different from the distribution of charged states in solution. We find that with increasing binding free energy the protonation shifts to higher pH values. However, NMR measurements did not show an appreciable difference in the chemical shifts for ligand solutions with and without QDs. This indicates that the distribution of charged states on QD does not deviate significantly relative to the ideal solution distribution.

To quantify the deviation between the theoretically computed distribution and the ideal solution distribution (see **Figure S7c**), we introduce three apparent $\mathrm{pK_a}$s that are associated with the various surface acid-base reactions. The apparent $\mathrm{pK_a}$s are defined by minimizing the deviation between the theoretical distribution and the distribution of charge ligands in dilute solution as a function of $\mathrm{K_a}$s. The distribution of the differently charged ligands in (infinite) dilute solution is given by the following equations:

$$g^{id}_{\mathrm{AHBH}} = \frac{[H^+]^2}{[H^+]^2 + (K_{a1} + K_{a2})[H^+] + (K_{a1}K_{a3})}, \text{and } g^{id}_{\mathrm{AHB}} = \frac{[H^+]K_{a1}}{[H^+]^2 + (K_{a1} + K_{a2})[H^+] + (K_{a1}K_{a3})}, \quad \mathbf{(S40)}$$

$$g^{id}_{\mathrm{ABH}} = \frac{[H^+]K_{a2}}{[H^+]^2 + (K_{a1} + K_{a2})[H^+] + (K_{a1}K_{a3})}, \text{and } g^{id}_{AB} = \frac{K_{a1}K_{a3}}{[H^+]^2 + (K_{a1} + K_{a2})[H^+] + (K_{a1}K_{a3})}. \mathbf{(S41)}$$

Mathematically, the deviation between the theoretical distribution and the distribution of charged ligands in an ideal, dilute solution is given by

$$\Delta = \sqrt{\sum_{k,pH} (g_k(pH, \{pK_{a,i}\}) - g^{id}_k(pH, \{pK^{Id}_{a,i}\}))^2}, \mathbf{(S42)}$$

Here the sum runs over the charged states $k = \{\mathrm{AHBH}, \mathrm{ABH}, \mathrm{AHB}, \mathrm{AB}\}$ of the PPA ligands and a number of pH values that range from 0 to 14 with increments of 0.1. $pK_{a,i}$ denotes the ideal solution of the PPA in solution. Its values are listed in **Table S2**. By minimizing Δ to the respect to pK_{a1}, pK_{a2}, and pK_{a3} we obtain a set of values for the

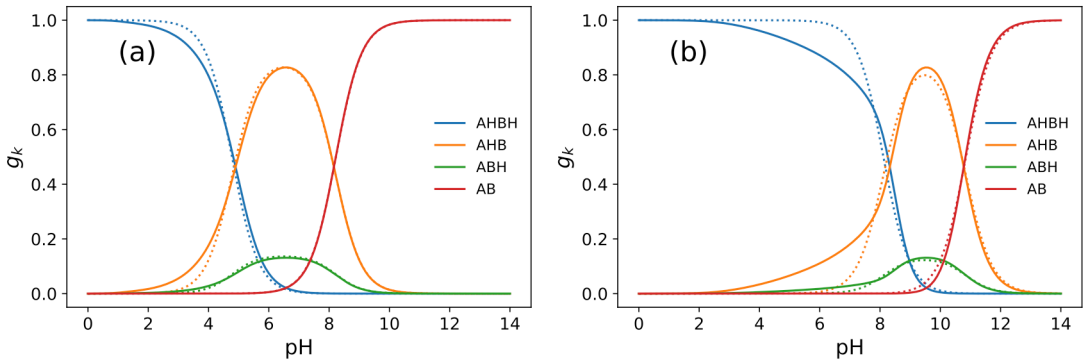

Figure S8. The fraction of ligands in their four differently charged, adsorbed states as function of pH for **(a)** a binding free energy $\Delta G^0 = -12\,k_BT$ and **(b)** $\Delta G^0 = -25\,k_BT$. The density of binding of sites is $\sigma = 5\,nm^{-2}$. The dotted lines correspond to curves obtained by fitting to ideal solution curves.

equilibrium constants that 'best' fit the ideal solution titration curves as given by **Eqs. S40** and **S31**. **Figure S8** shows some representative results of this procedure.

For intermediate binding free energies, the overall charge on the QD is small and the deprotonation of the adsorbed ligands follows approximately ideal solution behavior and are approximately perturbed as described by **Eqs. S40** and **S41** and therefore, $pK_{a,i} \approx pK_{a,i}$. For increasing binding free energies, the distribution of adsorbed states shifts to higher pH, thus $pK_{a,i} > pK_{a,i}$. Additionally, the shape of the distribution increasingly deviates from the ideal solution curves of **Eqs. S40** and **S41** $(\Delta\ \text{increases})$. Also, for small binding free energies the shape of the distribution increasingly deviates for ideal solution curves. The net positive charge leads to electrostatic interactions among the surface moieties that cause the distribution to deviate from the ideal solution curves. The NMR experiments indicate that the difference between the distribution of charged ligand states on the QD and in solution is small. Thus, the difference between the apparent pK_as of the adsorbed ligands and the ideal solution pK_as must be small. Therefore, there is a limit on the change in pK_a. Assuming that the measurements cannot differentiate between apparent pK_a and ideal solution pK_a that are less than 1, we find an upper bound for the binding free energies of $\Delta G^0 \geq -15.17 k_BT$, as can be read of from **Figure S9**, or equivalently a binding constant $K_b \leq 70k\,M^{-1}$. This binding free energy corresponds to the intermediate binding site density of $\sigma = 5\,nm^{-2}$. A binding site density of $\sigma = 8\,nm^{-2}$ yield $\Delta G^0 \geq -15.10\,k_BT$, while the low binding site density of $\sigma = 1\,nm^{-2}$ yields in $\Delta G^0 \geq -16.10\,k_BT$.

All of the above results pertain to the case in which the condensation free energy of the ions is set to have a weak value of $\Delta G^0 = -5\,k_BT$. Increasing this value to $-10\,k_BT$ for $\sigma = 5\,nm^{-2}$ did not result in appreciable changes of the upper bound of the ligand binding free energy. There are quantitative differences but qualitatively the QD systems behave similarly. Only for extreme low and high pH values and (very) weak

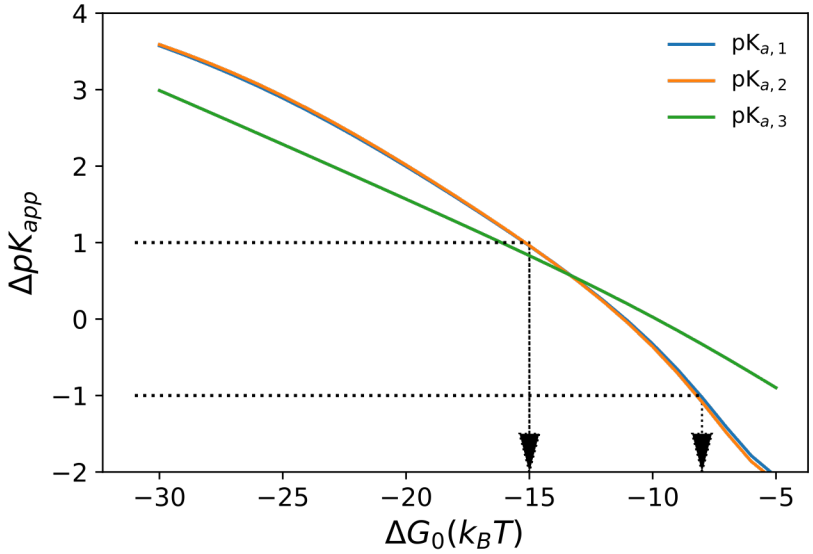

Figure S9. The difference in apparent $\mathrm{pK_a}$ as function of the binding free energy. The density of binding of sites is $\sigma = 5\ \mathrm{nm}^{-2}$. The dotted lines and arrows indicate the upper and lower bound. For completeness, the lower bound assuming $|\Delta pK_{app}| < 1$ is also presented. Observe that this lower bound is larger than the lower bound obtained from the assumption that the QD carries a negative charge. Hence this lower bound is ignored in favor of the more negative lower bound of ($\Delta G^0 \leq -10k_BT$).

ligand binding are there appreciable changes in the charge and amount. See also **Figure S7a**.

Finally, it should be pointed it out that our theoretical model involves a number of simplifying assumptions. We employed a generalized Poisson-Boltzmann approach that smeared out the surface charges, ignoring the discrete nature of the surface charges. Secondly and most notable, the surface of QD and its adsorption layer are modeled as a 2D-spherical surface. The surface topology and roughness and the finite size of the adsorption layer are not considered. The later effect can be taken into account by considering explicitly the volume of the adsorbed ligands, see e.g., Ref. 10.[11] Nonetheless, our theoretical model clearly indicates the large effect that pH has on the number of adsorbed PPA ligands and the charge of the QD. Effects of charge regulation at the QDs surface by adsorbing chemical moieties, such as PPA, that have ionizable charged states that are subject to acid-base equilibria need to be considered and cannot be ignored.

7. ADDITIONAL SUPPORTING FIGURES AND TABLES

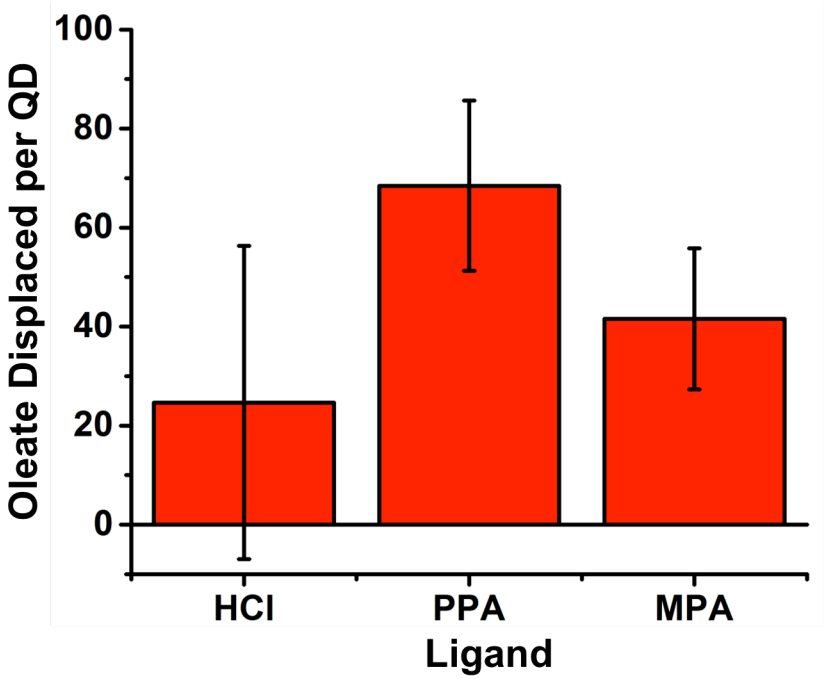

Figure S10. The number of oleate ligands displaced per QD in hexanes upon adding an isopropanolic aliquot of 150 eq. HCl or 300 eq. of PPA and MPA versus 5 µM oleate-capped CdSe and before the addition of DMF. The as-synthesized QDs initially have an oleate coverage of 276 ± 4 oleate ligands bound per QD.

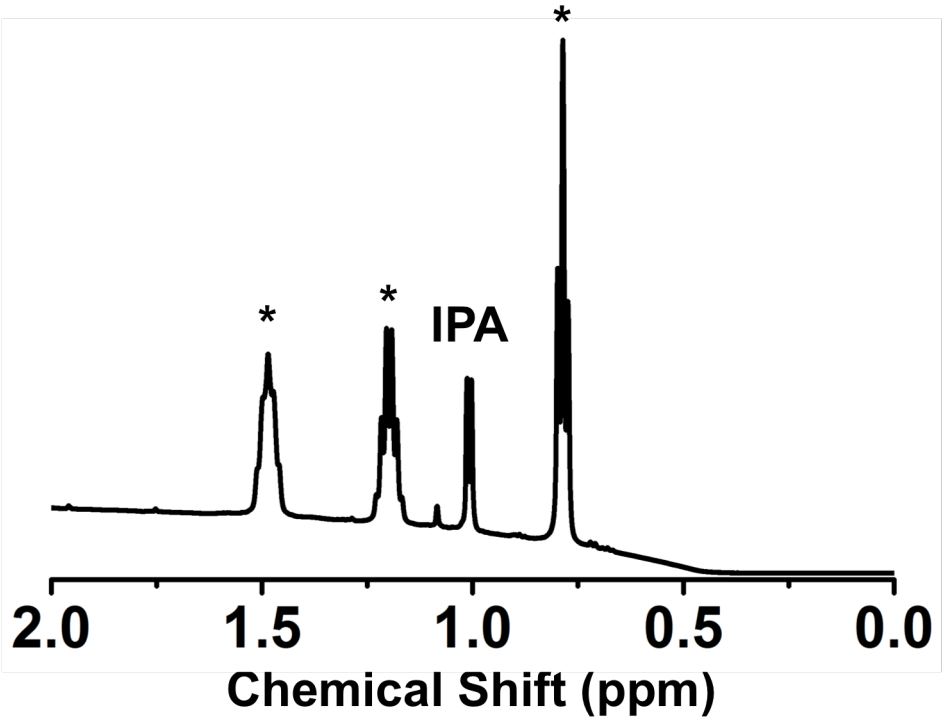

Figure S11. Representative spectrum of HCl-exchanged CdSe QDs in 90/10 (v/v) H_2O/ D_2O. The star indicates tetrabutylammonium chloride added as an integration standard and residual isopropanol (IPA) is also present in solution. The baseline increase is due to the high volume of H_2O relative to D_2O. No oleate signal is present in solution.

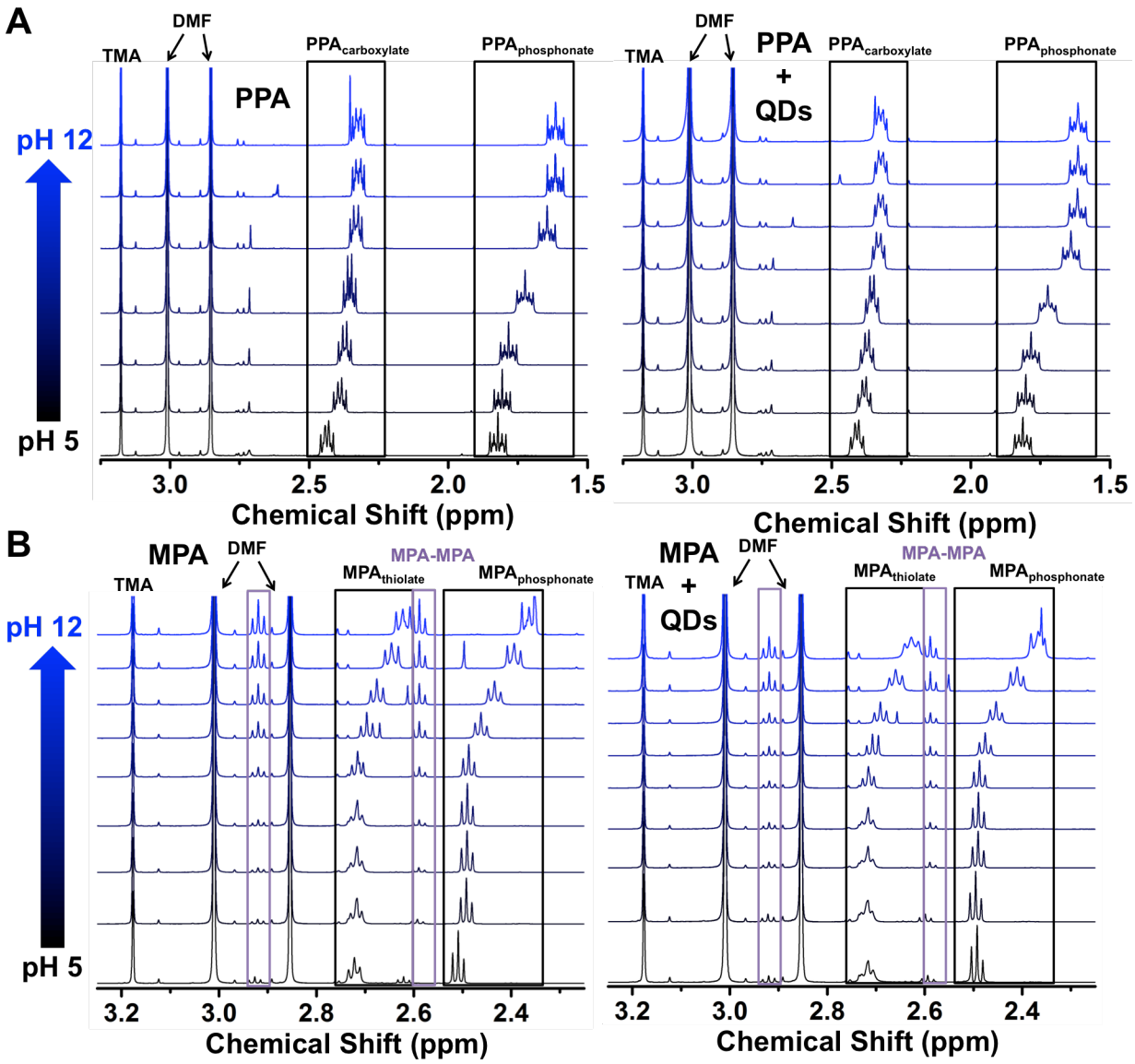

Figure S12. Stacked spectra of the chemical shift of both sets of alkyl protons of PPA **(A)** or MPA **(B)** as a function of pH with (right) and without (left) CdSe QDs in solution. Each sample contains 2 mM PPA or 1.8 mM MPA, and 0.4 mM tetramethylammonium nitrate as an integration standard in 80/20 (v/v) H_2O/ D_2O. The "w/ QDs" samples also contain 3.7 µM CdSe QDs **(A)** or 5.7 µM CdSe QDs **(B)**. The concentrations of the QDs in water vary due to the differential yield of phase transfer into water as a function of the ligand used for the exchange procedure. "TMA" indicates the tetramethylammonium protons and "MPA-MPA" indicates the disulfide formed by the oxidation of MPA in solution. The protons signals due to this disulfide are indicated with purple boxes in **B**.

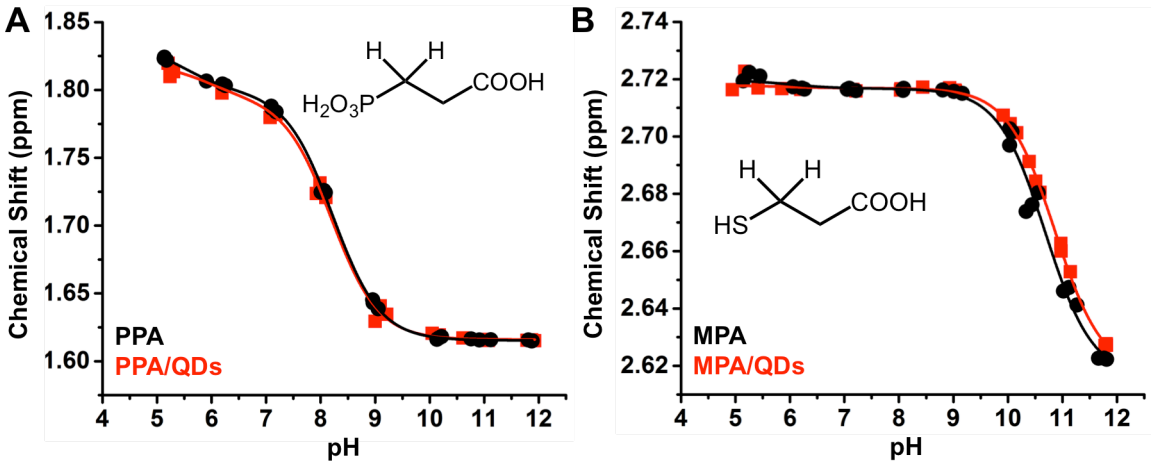

Figure S13. Plots of the chemical shift of one set of alkyl protons of PPA **(A)** or MPA **(B)** as a function of pH with (red) and without (black) CdSe QDs in solution. The insets show the measured concentrations of PPA or MPA in the corresponding samples. Each sample contains 2 mM PPA or 1.8 mM MPA, and 0.4 mM tetramethylammonium nitrate as an integration standard in 80/20 (v/v) H_2O/ D_2O. The samples with QDs also contain 3.7 µM CdSe QDs **(A)** or 5.7 µM CdSe QDs **(B)**. The concentrations of the QDs in water vary due to the differential yield of phase transfer into water as a function of the ligand used for the exchange procedure. The solid lines are fits using eq. S2, described below.

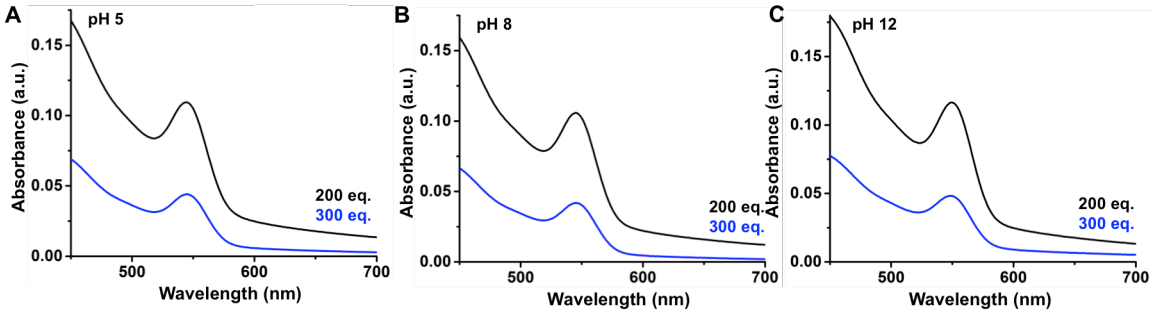

Figure S14. Plots of the absorbance spectrum with aliquots of equal volume of the resulting solution of CdSe exchanged with 200 or 300 equivalents of PPA at pH 5 **(A)**, or 8 **(B)**, or 12 **(C)**.

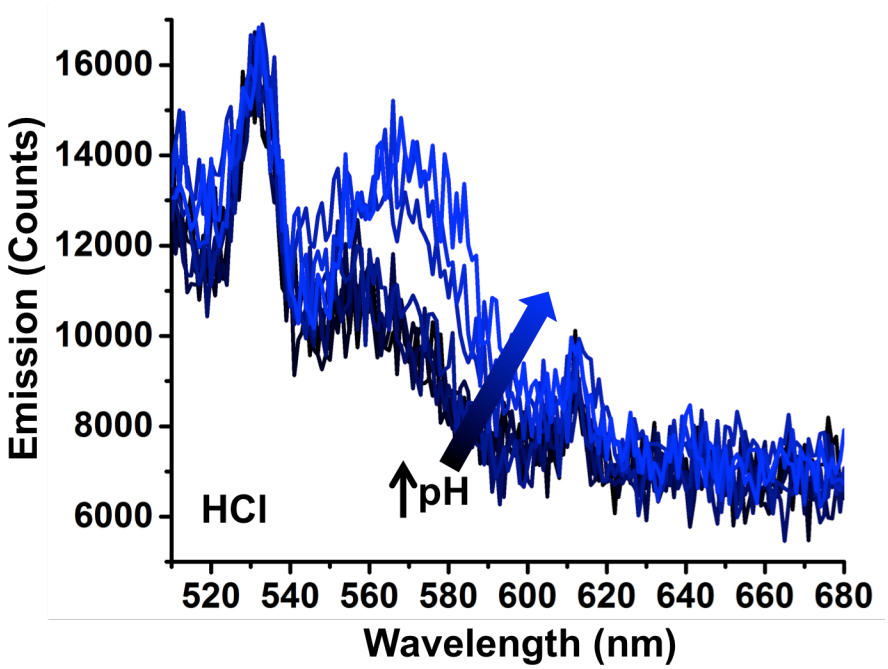

Figure S15. Emission spectra of 0.6 µM CdSe exchanged with 150 eq. of HCl. The arrow with the color gradient indicates the shifting of the spectra with increasing pH from pH 5 (black) to pH 12 (blue).

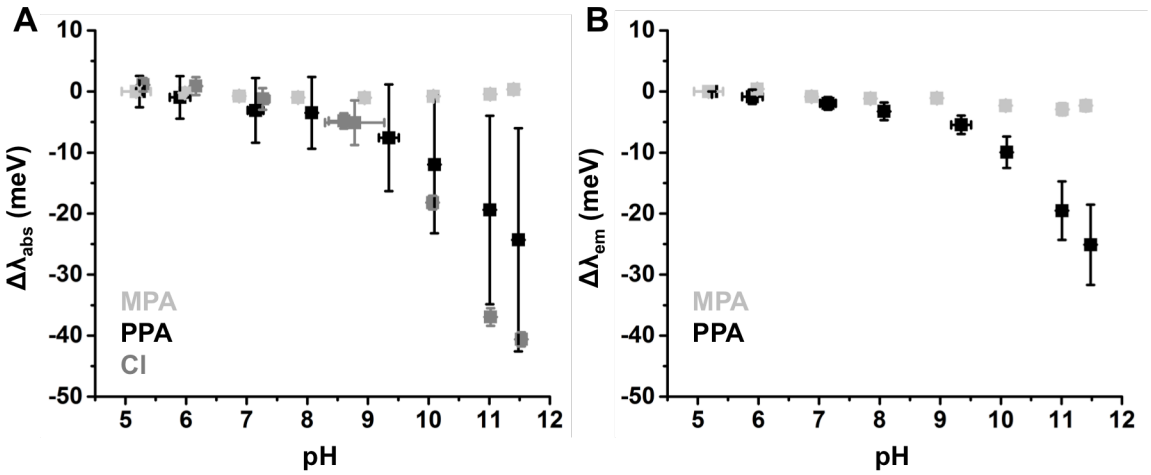

Figure S16. The magnitude of the shift of λ_{abs} **(A)** and λ_{em} **(B)** of 0.7 µM CdSe with 300 equivalents of MPA (black), 0.6 µM CdSe with 300 equivalents of PPA (dark gray), and 0.6 µM CdSe with 150 equivalents of Cl^- (light gray) as a function of pH. The HCl-capped QDs were non-emissive. Each data point represents the average of at least three samples at each pH where each sample was adjusted individually to the desired pH.

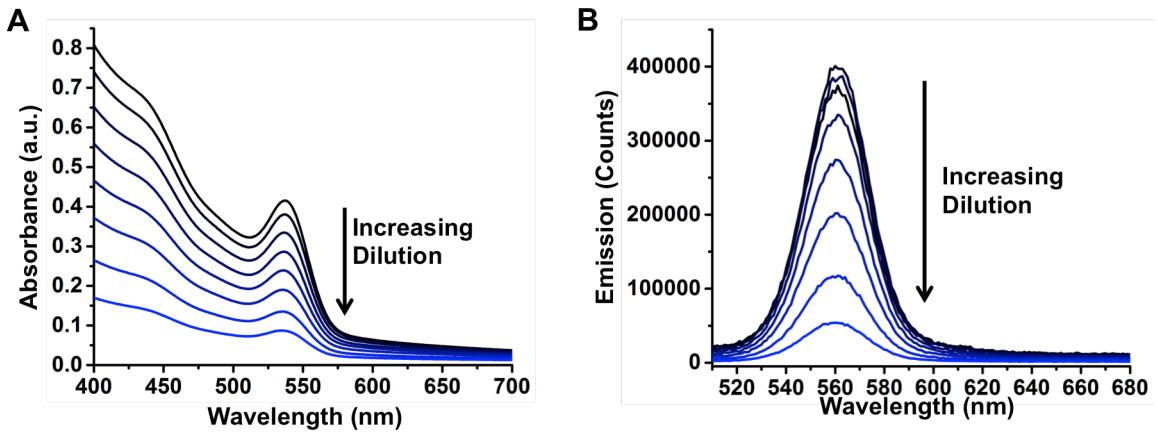

Figure S17. Ground state absorbance **(A)** and emission **(B)** of CdSe QDs exchanged with 300 equivalents of PPA upon dilution from 5.1 µM to 1.3 µM.

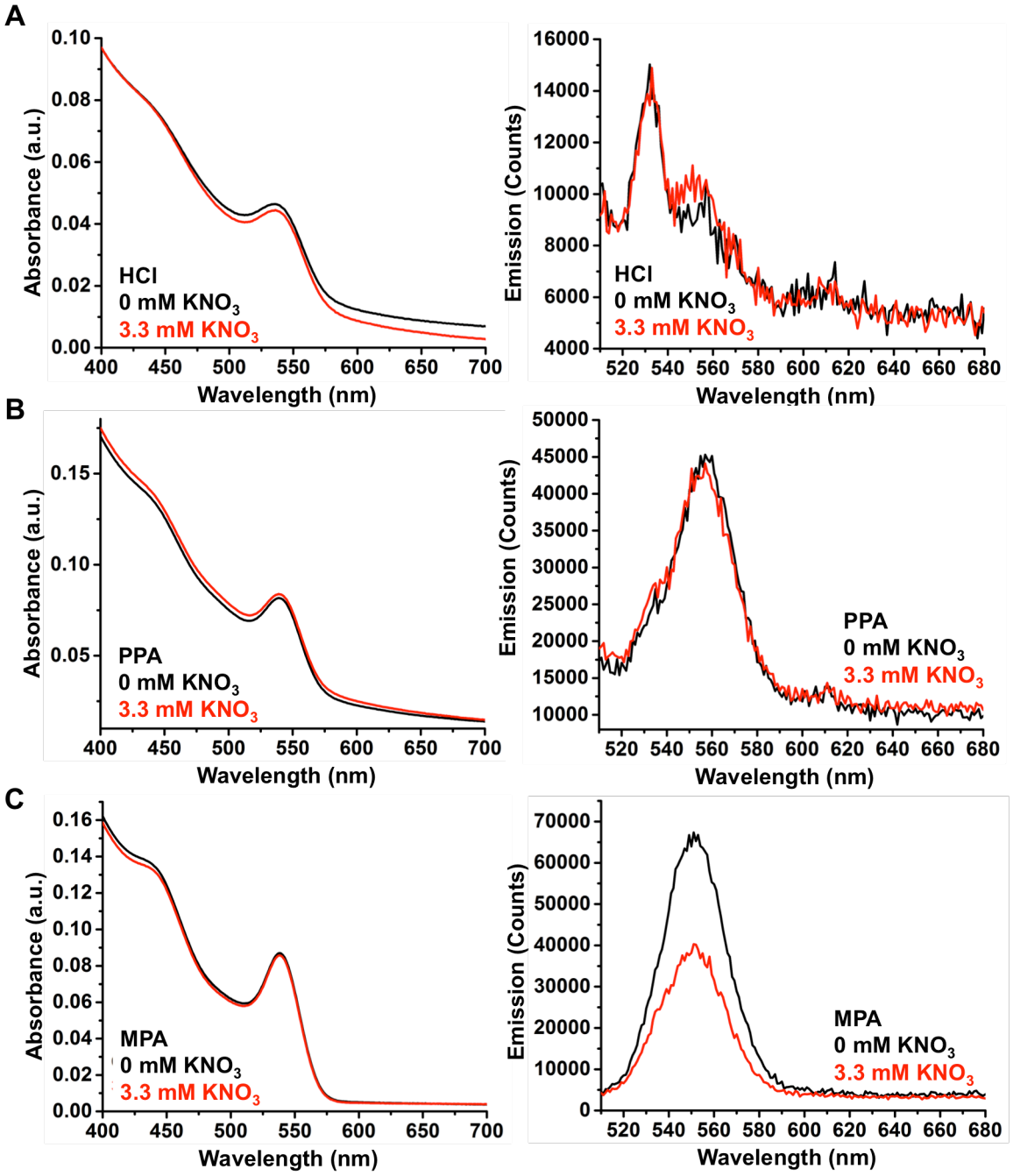

Figure S18. The shift in the ground state absorbance (left) and emission (right) of CdSe QDs exchanged with 150 eqivalents of HCl **(A)**, 300 equivalents of PPA **(B)**, and 300 equivalents of MPA **(C)** upon the addition of 3.3 mM KNO_3 at pH 7. Absorbance spectra are corrected for dilution, and emission spectra are corrected for absorbance at the excitation wavelength. The QDs do eventually precipitate at high salt concentration (> 0.1 M), which inhibits our ability to continually cycle the pH in **Figure 2A** of the main text.

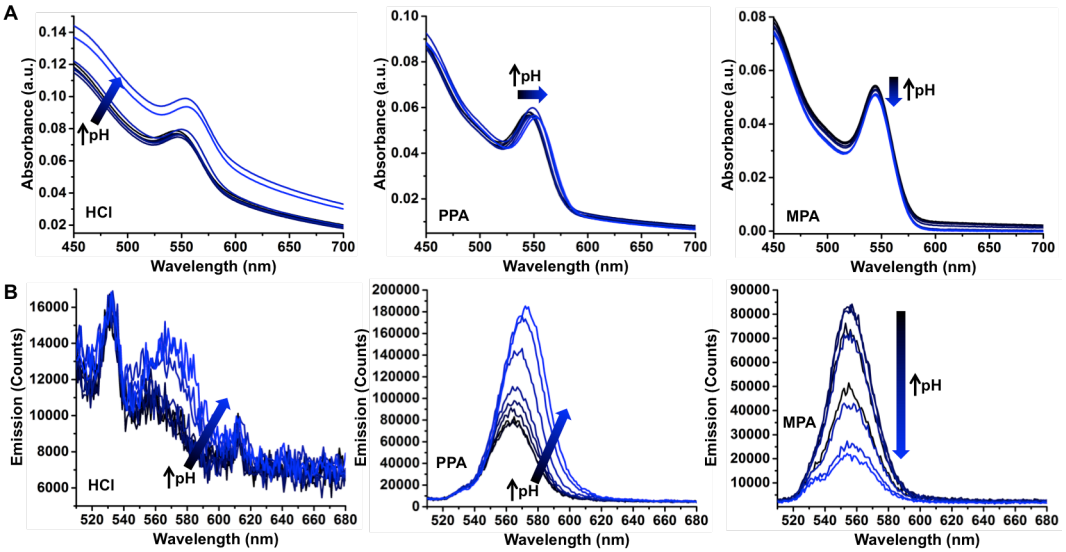

Figure S19. Representative absorbance **(A)** and emission **(B)** spectra as a function of pH with HCl- (left), PPA- (center), and MPA-exchanged (right) CdSe QDs in solution. The samples contain 0.6 µM CdSe with 150 eq. of HCl, 0.6 µM CdSe with 300 eq. PPA, or 0.7 µM CdSe with 300 eq. MPA. The concentrations of the QDs in water vary due to the differential yield of phase transfer into water as a function of the ligand used for the exchange procedure. The arrow with the color gradient indicates the shifting of the spectra with increasing pH from pH 5 (black) to pH 12 (blue). We attribute the decrease in baseline absorbance with increasing pH to increasing electrostatic repulsion between QDs that results in the breaking up of small aggregates in solution. We attribute the increasing photoluminescence intensity of PPA-exchanged QDs to increasing passivation of the CdSe surface by hydroxide ions with increasing pH, as described in the main text. We attribute the decreasing photoluminescence intensity of MPA-exchanged QDs with increasing pH to the thiol-thiolate equilibrium of the MPA ligand, as has been previously described.[1] We also confirm that the average standard deviation of the λ_{abs} or λ_{em} between samples prepared at the same pH is only 15-16 % of the total magnitude of the optical shifting induced by pH variation that we observe in **Fig. 1** for the HCl-exchanged QDs and PPA-exchanged QDs.

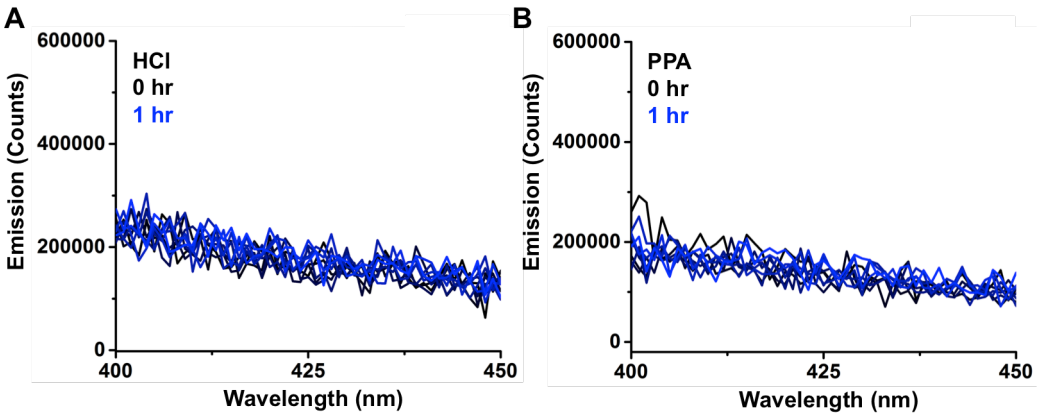

Figure S20. The emission spectra from 0 minutes (black) to 1 hour (blue) of 2 mM terephthalic acid with **A)** CdSe QDs exchanged with 150 equivalents of HCl or **B)** CdSe QDs exchanged with 300 equivalents of PPA. The solution pH is 12 for the data in both **A** and **B**.

8. REFERENCES

1. S. Jeong, M. Achermann, J. Nanda, S. Ivanov, V. I. Klimov and J. A. Hollingsworth, *Journal of the American Chemical Society*, 2005, **127**, 10126-10127.
2. R. Calzada, C. M. Thompson, D. E. Westmoreland, K. Edme and E. A. Weiss, *Chemistry of Materials*, 2016, **28**, 6716-6723.
3. O. Chen, X. Chen, Y. Yang, J. Lynch, H. Wu, J. Zhuang and Y. C. Cao, *Angewandte Chemie International Edition*, 2008, **47**, 8638-8641.
4. M. R. J. Nor Aliya Hamizi, *Int. J. Electrochem. Sci.*, 2012, **7**, 8458-8467.
5. W. W. Yu, L. Qu, W. Guo and X. Peng, *Chemistry of Materials*, 2003, **15**, 2854-2860.
6. K. O. Aruda, V. A. Amin, C. M. Thompson, B. Lau, A. B. Nepomnyashchii and E. A. Weiss, *Langmuir*, 2016, **32**, 3354-3364.
7. A. I. P. Pierre-Henri C. Heubel, *Journal of Solution Chemistry*, 1979, **8**, 615-625.
8. L. Protesescu, M. Nachtegaal, O. Voznyy, O. Borovinskaya, A. J. Rossini, L. Emsley, C. Copéret, D. Günther, E. H. Sargent and M. V. Kovalenko, *Journal of the American Chemical Society*, 2015, **137**, 1862-1874.
9. M. D. Donakowski, J. M. Godbe, R. Sknepnek, K. E. Knowles, M. Olvera de la Cruz and E. A. Weiss, *J. Phys. Chem. C*, 2010, **114**, 22526-22534.
10. R. J. Nap, M. Tagliazucchi, E. Gonzalez Solveyra, C.-l. Ren, M. J. Uline, I. Szleifer, O. Azzaroni and I. Szleifer, 2017.
11. D. Wang, R. J. Nap, I. Lagzi, B. Kowalczyk, S. Han, B. A. Grzybowski and I. Szleifer, *J. Am. Chem. Soc.*, 2011, **133**, 2192-2197.
12. R. J. Nap, A. Lošdorfer Božič, I. Szleifer and R. Podgornik, *Biophys. J.*, 2014, **107**, 1970-1979.
13. M. A. Carignano and I. Szleifer, *J. Chem. Phys.*, 1995, **102**, 8662-8669.

14. J. Schwinger, J. DeRaad, L. L., K. A. Milton and W.-Y. Tsai, *Classical Electrodynamics*, Persus Books, Reading Massachusetts, 1998.
15. R. Nap, P. Gong and I. Szleifer, *J. Polym. Sci., Part B: Polym. Phys.*, 2006, **44**, 2638-2662.
16. R. J. Nap, M. Tagliazucchi and I. Szleifer, *J. Chem. Phys.*, 2014, **140**, 024910.
17. S. Donnini, A. Villa, G. Groenhof, A. E. Mark, R. K. Wierenga and A. H. Juffer, *Proteins: Structure, Function, and Bioinformatics*, 2009, **76**, 138-150.
18. L. E. Davis, *J. Phys. Chem.*, 1945, **49**, 473-479.
19. N. Z. Misak, *React. Polym.*, 1993, **21**, 53-64.
20. T. Markovich, D. Andelman and R. Podgornik, *Europhys. Lett.*, 2017, **120**, 26001.
21. A. C. Hindmarsh, P. N. Brown, K. E. Grant, S. L. Lee, R. Serban, D. E. Shumaker and C. S. Woodward, *ACM Trans Math Software*, 2005, **31**, 363-396.